Wind effect on bottom shear stress, erosion and redeposition on Zostera noltei restoration in a coastal lagoon; Part 2

Elena Alekseenko, Bernard Roux

Wind effect on bottom shear stress, erosion and redeposition on *Zostera noltei* restoration in a coastal lagoon; part 2

E. Alekseenko[a,b,*], B. Roux[c]

[a] Shirshov Institute of Oceanology, Russian Academy of Sciences, Nakhimovsky Prospekt 36, 117997, Moscow, Russia

[b] Laboratoire des Sciences du Climat et de l'Environnement (LSCE/IPSL), CEA Saclay, Gif-sur-Yvette, 91191, France

[c] Aix-Marseille Université, CNRS, Centrale Marseille, M2P2 UMR 7340, 13451, Marseille, France

*Corresponding author: E. Alekseenko, lena.alekseenko@gmail.com

Abstract

This paper concerns wind effect on bottom shear stress (BSS), resuspension and redeposition of bottom sediments in the nearshore areas of the Etang de Berre (EB), a semi-enclosed lagoon, in the context of Zostera noltei (Z.n.) restoration. As in our previous paper, the first step is to compare BSS with its threshold, BSS_{cr}, for a wind speed of 21 m/s. But, here, a new simulation is performed for 16 wind directions regularly spaced. It permits to analyze the combined effect, over one year, of these winds on the erosion risk. For that, a mean value of $|BSS|$, i.e., a weighted average based on the frequency of each wind directions, has been determined and compared to BSS_{cr} for a class of roughness parameters. A similar averaging of $\overrightarrow{BSS}$ has been also evaluated to obtain the direction of an average bottom current.

Then, the most important contribution of the present paper concerns the modelling of the wind-induced sediment erosion, transport and redeposition. The specific module SEDIM/MARS3D is used to determine how the thickness of a given mud-sand sedimentary layer can be changed by the wind-induced current during typical periods of 3 days of constant wind. This numerical study is performed for three wind speeds in the two main wind directions: N-NW and S-SE. The time evolution of this initial sedimentary layer permits to determine where and when the erosion would be large enough to be a stressor for the Z.n. restoration.

For an extreme erosion rate of 10^{-3} kg/m²/s, for a strong wind speed of 21 m/s and an initial sedimentary layer of 15cm, all this layer would be eroded in several nearshore areas after 3 days. The erosion risk is maximum along the eastern shore, where an additive effect of the two opposite winds can be expected. Indeed, S-SE and N-NW winds create coastal jets of opposite direction and of about the same intensity exerting alongshore erosion and deposition at about the same places.

The present results concerning the time evolution of erosion depth induced by the wind improve our knowledge of the erosion risk on the Z.n. restoration in EB. They will be useful to appropriately orient the action of politics and managers for a future restoration program.

1. Introduction

The present work is an extension of a recent numerical study (Alekseenko et al., 2017) devoted to the restoration of *Zostera noltei* (Z.n.) – an intertidal dwarf-eelgrass - in the Etang de Berre (EB) which is one of the largest Mediterranean lagoon in South of France. The massive loss of submerged aquatic vegetation (SAV), all along the coastal ocean, is a common

worldwide ecological problem. The conservation and restoration of seagrass meadows provide a strategy to mitigate climate change while conserving these important ecosystems (Duarte et al., 2013). Concerning Z.n. meadows in EB, they are specially protected as they also provide habitats and feeding grounds for migratory birds (Natura 2000).

Concerning Z.n. meadows in EB, it is mentioned by Warner (2012) that they were severely destroyed in the last fifty years due to anthropogenic water pollution and huge amount of silt and freshwater outflow from a hydroelectric power plant built in 1966. But, during the last decade, the hydropower outflow and silt amount were reduced and regulated, and resilience of Z.n. meadows were observed in situ during the last four years by divers of a non-profit association (Bazile, 2015; Bazile, 2017), in several areas very close to the shoreline. These observations are very promising as the divers confirm that these meadows are now increasing year after year (Bazile, 2017).

Z.n. – to be restored in EB - are marine flowering plants having a root and rhizome. They generally colonize soft substrates (mud-sand) which can be easily eroded by the bottom shear stress. The critical level of burial or erosion tolerated by this species is extremely low (between 4 and 8 cm) due to the small size of the species and the lack of vertical rhizomes (Cabaço & Santos, 2007). These limits concerning resilience of Z.n. to burial or erosion disturbances are experimentally confirmed by a more recent work by Han et al., (2012).

In our previous numerical study, the MARS3D numerical model was used to analyze the 3D current, salinity and temperature distribution induced by three meteorological, oceanic and anthropogenic forcings in this lagoon (Alekseenko et al., 2017). We have also analyzed the complex hydrodynamics due to the tide effect in the Caronte channel connecting EB to the sea (Alekseenko & Roux, 2017).

In the previous study, which was realized for large values of the dominant wind in N-NW direction, the main contribution concerned the bottom shear stress (*BSS*) fields in the nearshore areas, for different values of the bottom roughness parameter. Then, the *BSS* values were compared with the critical *BSS* at which the mobility of such bottom sediments would occur.

As it is mentioned by Berlamont & Torfs (1996), experimental research on the erosion of mixed sediments (Torfs, 1994, Williamson & Torfs,1996) showed an increasing erosion resistance with increasing content of cohesive material.

- When the mixture only contains a very small amount of cohesive material the fines (i.e., the fraction smaller than 63 μm) are washed out of the surface layer at very low values of the bed shear stress, lower than the critical shear stress needed to move the sand particles.

- Adding more cohesive material, the fines fill the pore spaces in between the sand grains and make the mixture smoother and thus more difficult to erode. Such a reduction of the erodibility of mud-sand mixtures is also reported by Panagiotopoulos et al. (1997) when mud is added up to 50 % to two sorts of sand: 150 microns and 215 microns; their experiments showed that BSS_{cr} would be increased of about 50 % and 100 %, respectively.

Panagiotopoulos et al. (1996) recommend, when the shear strength (i.e. threshold of movement) of natural marine sand-mud deposits has to be investigated, to consider the modelling with caution. Indeed, it would be needed to consider the type of clay minerals, pH and temperature of the eroding (ambient) fluid, the chemical properties of the pore and eroding fluids, internal sediment structure, degree of sediment saturation and biological activity. But, such properties are very specific of any coastal hydro-system (lagoon or estuary); and we do not have such a detailed knowledge for EB.

A detailed overview of previous sediment transport modelling is given by Dufois & Le Hir (2015):

- Chesher & Ockenden (1997) solve transport equations for sand and mud concentrations, with contrasted settling velocities. Interactions are accounted for by considering the same critical erosion shear stress for sand and mud, which depends on the mud content in the bed.
- Van Ledden (2002) also consider two sediment fractions (sand and mud), both transported in suspension, and distinguish two regimes (non-cohesive and cohesive) in the formulation of erosion, depending on the mud content in the surficial sediment.
- Le Hir et al. (2011) propose a modelling strategy applied to the suspended transport of sand and mud mixtures, and which accounts for consolidation of mixed sediments. The model state variables are the different classes of particles, generally classified according to their size, and grouped into categories that are either transported as bedload or in suspension. The bed is described as thin layers characterized by a distribution of these classes.
- A more recent and very exhaustive review concerning modelling and measurement of critical bed-shear stress for sand-mud mixture has been presented by van Rijn (2016). It confirms the extreme diversity of the behavior of cohesive sediment (due to biogenic effect in particular), and the extreme variety of the critical bed-shear stress data obtained in-situ and/or in flumes. That means that it is extremely difficulty to derive some general law to express BSS_{cr} as function of particle size for example.

Amos et al. (2010) in their paper devoted to erosion rate of cohesive sediments in Venice lagoon pointed out the importance of the erosion rate per unit area of bed flux, E, which is an essential precursor to the prediction of eroded depth and the suspended sediment concentration for a given applied bed shear stress. Whilst solution of the erosion threshold is often reported, the evaluation of the variation of this threshold through the process of erosion (eroded depth) is usually omitted or not estimated. The field experiments of Amos et al. (2010) showed that E is changing throughout the period of a given applied shear stress. The maximum rate increases with stress; but the minimum rate appears roughly constant (about 10^{-4} kg/m^2/s) for the mud-sand sediment in several stations in Venetian northern and southern lagoons: (13% sands, 61% silts, 26% clays) and (16% sands, 54% silts and 30% clays), respectively (after Tab.2 of Amos et al.,2010). Note that this sediment composition is not far from that measured by Rigaud (2011) in the central part of EB.

In areas with high wave exposure and strong currents, seagrass may be damaged due to excessive sediment transport, which does not allow seeds to become established, or eroding/burying existing seagrass beds. As a result, wave- or current-exposed areas tend to have patchy seagrasses or are unvegetated (Fonseca & Bell 1998). An intermediate flow regime may be optimal for seagrass growth and development.

Interactions between seagrasses and water flow in their natural environment when exposed to wind-driven currents, tides and waves have been intensively studied by Koch et al. (2006). Kombiadou et al. (2014) have also investigated the effects of an abundant vegetation to the near-bed hydrodynamics and to the sediment suspension in the Arcachon lagoon. They show that Z.n. meadows play an important role to velocity attenuation and to sediment stabilization, with flow and suspended sediment concentrations damping, compared to an unvegetated state. In the today state, the Z.n. meadows in EB are so sparse that our present modelling does not consider velocity attenuation by the vegetation.

The present study contains two main parts. The first part is still devoted to the wind effect on *BSS* fields, but here we consider 16 wind directions; the frequency of which are given from a weather data base shown in Fig.2 (after SOGREAH, 2003). In the second part, a specific sediment module of MARS3D (called SEDIM) is used to simulate the erosion and the transport of fine bottom sediments (mud and sand) which are initially uniformly distributed. The goal is

to evaluate the risks to get of profound erosion and to get some scouring of lighter sediments that would be redeposited further afield; which would be deleterious for Z.n. restoration. SEDIM module is described in Subsection 3.4 and is used in Section 5.

2. Study site

EB has been under intense anthropogenic pressure for several decades (Warner, 2012). At the middle of the 20th century, Zostera meadows occupied over 6000 ha. But subsequently, the lagoon was disturbed by urban and industrial pollution, and since 1966 by a hydropower station leading to a very large increase of freshwater and silt inflow. Bernard et al. (2007) confirmed the near extinction of Zostera in EB and mentioned that it was probably resulting from several causes, namely, pollution (including nutrients), low salinity and turbidity resulting from huge amounts of water and silt from hydropower station.

To alleviate the hydropower disturbance to Z.n., the annual hydropower runoff is reduced to 1.2×10^9 m^3, since 2005. In addition, the maximal amount of silt associated with this annual runoff is limited to 60 000 tons.

In Fig.1, we show four control areas (PA, PB, PF, PM) in the Grand Etang which correspond to the places where benthic vegetation existed 50 years ago and then disappeared completely (PF and PM, at the western shore) or partially (PA and PB, at the eastern shore). They also correspond to the main places which were initially considered for a replanting program, after this final hydropower regulation, as mentioned by Bernard et al. (2007). This replanting attempt was not successful; this is the main reason for which our numerical studies were focused on understanding the possible role of the bottom shear stress, which depends on the bottom granulometry, and salinity, in these four places.

A large part of EB bottom is composed of mud and fine sand carried for several decades from rivers and the sea. The granulometric distribution of sediments in two places in EB have been measured by Rigaud (2011). In both cores, sediments are constituted of silts (51-81%) and clays (13-28%). Fine sands were also found but in proportions always less than 20%. The fraction larger than 2 mm which corresponds to shell residues exists only in some parts but always less than 15% in mass. The granulometry in the fraction in which the analysis has been performed is constant along the profiles in both cores (silts: about 81% in Grand Etang and about 85% in Etang de Vaïne).

Salinity and temperature measurements are reported by Delpy et al. (2012) from three permanent moorings in the Grand Etang (SA1 in the north, SA2 in the middle and SA3 in the southern part) equipped with five multiparametric probes, CTD SBE37 (Seabird), placed at five depths (see Tab.1 of Delpy et al., 2012). These experimental results exhibit an almost uniform salinity in the vertical direction (i.e. no haline stratification), but with a periodic seasonal evolution: around 25 PSU in the summer time and less than 15 PSU in the winter time where the largest hydropower runoffs are used. These vertical profiles of salinity and temperature have been used to carefully validate our numerical model in a real situation, for a one-year period, from May 2009 to May 2010 (Alekseenko et al., 2017).

One conclusion of our previous work is that the salinity conditions in EB after the last operational regulation of the hydropower runoff (in 2005) is not a stressor for the SAV replanting and resilience (Alekseenko et al., 2017). So, the present work is mainly devoted to complement the previous study about wind effect on *BSS* (in Section 4) and to study the time evolution of erosion and deposition induced by strong winds (in Section 5).

3. Model description

The numerical model concerns the 3D currents due to the three dynamical forcings: sea

tide and freshwater runoff (with the consequent baroclinic pressure gradient) and strong wind.

The present study is realized with MARS3D developed by IFREMER (Lazure & Dumas, 2008; Lazure et al.,2009). MARS3D contains a hydrodynamical model based on the governing equations proposed by Blumberg & Mellor (1986). It is based on the system of incompressible Reynolds Averaged Navier-Stokes equations in the classical Boussinesq approximation with the hydrostatic assumption.

The surface elevation, η, is represented by $z = \eta(x, y, t)$, and the bottom relief, H, by $z = -H(x, y)$. MARS3D uses a coordinate transformation "sigma" to permit a better resolution near the two boundary layers (at the surface and at the bottom). The water column is divided into layers in the transformed vertical "sigma" coordinate: $\sigma = (z - \eta)/(H + \eta)$; varying from -1 at the bottom to 0 at the free surface.

EB bathymetry obtained from the marine map NAVICARTE 505 of SHOM "Port-Saint-Louis-du-Rhone; Marseille/étang de Berre" using image recognition algorithm have been considered in the present numerical modelling. The numerical aspects of EB configuration and its hydrodynamic simulation were described in Alekseenko et al. (2013a,b) where the effects of refinement of the sigma-grid on the computed velocity fields were examined in order to choose an optimal grid for appropriate accuracy and acceptable computational time.

3.1. Boundary conditions

For the dynamical governing equations, the boundary conditions are the ones used by Alekseenko et al. (2013 a). The horizontal components of surface stress from wind, and of bottom friction are imposed as follows:

- for the surface stress components $(\tau_{s,x}, \tau_{s,y})$

$$(\tau_{s,x}, \tau_{s,y}) = \rho_a C d_s \|\underline{V}_{10}\|(U_{10}, V_{10}),$$ (1)

where $\underline{V}_{10} = (U_{10}, V_{10})$ is the wind velocity 10 m above the lagoon surface, $\rho_a = 1.25$ kg/m³ is the air density, $C d_s$ is the surface drag coefficient.

- for the bottom stress components $(\tau_{b,x}, \tau_{b,y})$

$$(\tau_{b,x}, \tau_{b,y}) = \rho_0 C d_b \|\underline{V}\|(U, V)$$ (2)

with

$$C d_b = \left(\kappa / \ln \left(\frac{z + H + z_0}{z_0}\right)\right)^2,$$ (3)

where $\underline{V}$ is the velocity vector with horizontal components (U, V), $C d_b$ is the bottom drag coefficient, $\kappa = 0.4$ is the Von Karman constant, ρ_0 is the reference density ($\rho_0 = 1015.27$ kg/m³; corresponding to a salinity of 20 PSU and a temperature of $10^o C$), $z_0 = 0.0001$ m is the bottom roughness (corresponding to coarse sand).

At surface ($\sigma = 0$) and at bottom ($\sigma = -1$), boundary conditions for temperature and salinity are:

$$\rho_0 \nu_H \left(\frac{\partial T}{\partial \sigma}, \frac{\partial S}{\partial \sigma}\right) = (0,0),$$ (4)

where ν_H is the vertical eddy viscosity.

For more details about the boundary conditions, and the meshing strategy the reader can see our last paper (Alekseenko et al., 2017).

3.2. Equation of state

As described in Lazure & Dumas (2008), in the MARS3D model, the dynamic equations

are solved together with transport equations for salinity (S) and temperature (T). These transport equations are coupled with the dynamic equation through buoyancy and are solved in a way consistent with the mass conservation solver in order to be mass preserving, not only for water but also for any tracer.

The density ρ is a mathematical function of temperature, salinity, and pressure. MARS3D includes the 1980 Equation of state, abbreviated EOS80.

3.3. Sediment transport

Exhaustive review of several works devoted to transport and fate of fine, cohesive sediments, and the exchange of fine sediment between the sea bed and the water column above have been given by Winterwerp et al. (2012) and by Van Rijn (2016). It concerns in particular the shear flow-induced erosion of soft cohesive sediments beds, for which they suggest to distinguish three types of erosion of muddy beds, as follows:

- floc erosion, which is the pick-up of individual particles and small-scale flocs of the top layer (millimeters) of the bed by the turbulent vortices of the fluid flow just above the bed, and which occurs for $0.5BSS_{cr}<BSS<1.5BSS_{cr}$ with BSS_{cr} - erosion threshold stress and BSS - applied time-averaged bed-shear stress; some erosion may already occur for $BSS<BSS_{cr}$ due to higher turbulent stresses;
- surface erosion for $1.5BSS_{cr}<BSS<3BSS_{cr}$, which is the simultaneous mobilization of several layers of particles and flocs.
- mass erosion $BSS>3BSS_{cr}$, which is the erosion of lumps of bed material when the applied fluid stresses are larger than the undrained soil strength of the bed.

Concerning the modeling of transport sediment in semi-enclosed areas, such as EB, where it is generally necessary to consider both sandy and muddy sediments, we will use the sediment module coupled with MARS3D model (called SEDIM) provided by IFREMER (Le Hir et al, 2011; Cayocca et al, 2014).

MARS3D model manages particle advection in the water column, according to a depth-averaged formulation or to a 3D framework, whereas SEDIM module manages particle settlement in the water column as well as exchanges with the bed by erosion, deposition, and consolidation processes in the bed. In SEDIM module, processes such as deposition on bed sediment and erosion are modelled for each horizontal cell (dx*dy) separately (1D model, see Fig.5 in Cayocca et al, 2014), with a variable number of layers whose thickness, porosity and concentration vary with time by sedimentation and resuspension events.

The modelling techniques in sediment transport simulations are split into two classes (Le Hir et al., 2011):

- "for non-cohesive sediment (sand and gravel), sediment evolution is computed by solving a continuity equation (Exner equation) where erosion or deposition result from the divergence of a transport capacity related to the hydrodynamic regime; this method is suitable when equilibrium is reached rapidly, which is the case for sediment with high settling velocity;
- for fine sand and mud that are mostly transported in suspension, an advection/diffusion equation is solved (either depth-integrated or not) and the sediment evolution is straightforwardly deduced from erosion and deposition rates".

Le Hir et al. (2011) described in detail the sediment transport modelling strategy which offers the possibility to account: simultaneous bed load and suspended sediment transport, mixing of several sediment classes in the water column as well as in the sediment, consolidation of muddy and mixed sediments with possible segregation of sand particles by adapting Gibson

theory, management of erosion fluxes depending on the cohesive or non-cohesive nature of the superficial sediment. Special attention was paid to the way the sediment layers content is updated after deposition, in order to simulate possible pore filling up between large particles in superficial sediment before creating a new layer".

According to Le Hir et al. (2011), the suspended transport is computed by solving an advection-diffusion equation (6) for the concentration of different particle classes which are grouped into three types defined by their behavior:

- "coarse type, generic for non-cohesive particles that are transported as bedload only: it is normally affected to coarse sand, and can be extended to gravels, cobbles and pebbles;

- sand type, generic for non-cohesive particles that are transported in suspension: it refers to fine sand, but also to medium sand, since the possibility to simulate transport capacities through an advection-diffusion process has been demonstrated (Waeles et al., 2007);

- mud type, generic for cohesive particles; these are naturally transported in suspension but are also likely to flocculate (inducing a variation of settling velocity) and to undergo consolidation in the bed; the mud type is usually affected to silt and clay but could also be used for organic matter".

$$\frac{\partial c}{\partial t} = -\frac{\partial c u_i}{\partial x_i} + \frac{\partial c W_s}{\partial z} + \frac{\partial}{\partial z}\left(K_z \frac{\partial c}{\partial z}\right) + E - D \qquad (5)$$

Where c - sediment concentration in water, W_s - particle settling velocity, K_z - coefficient of vertical turbulent exchange, E - erosion flux and D - deposition flux.

The erosion flux for mixed sediment is taken from Le Hir et al. (2011). It is proportional to the erosion rate E_0 and it involves critical erosion bottom shear stresses: τ_{es} for sand, and τ_{em} for mud (see their equations 1 and 2). It is recalculated from Shields approach technique at each time step from taking into consideration fractions of a mixed sediment (see their Fig.3).

For the deposition flux the formulation given by Le Hir et al. (2011, see their equation 3) is used. It depends on particle settling velocity W_s and on critical deposition bottom shear stress which, following Winterwerp (2007), is taken as BSS_{cr}.

A major difficulty for implementing the model is the choice of the state variables, since natural size-spectra are often continuous and the computation cost increases with the number of state variables. The values of all the needed parameters for our numerical experiments (W_s, E_0, BSS_{cr}, etc) are given in Section 5.1.

3.4. Description of model scenarios

As in our previous numerical study (Alekseenko et al., 2017), different scenarios are considered. In the first scenario (scen.#1), in absence of wind and starting from an initial homogeneous distribution of salinity (S=20 PSU) and a flow at rest, we obtain a stratification process (after 14 days) under the influence of two dynamical forcings: a seawater influx of high salinity (38 PSU) and a freshwater inflow produced by the hydropower station and two rivers. The aim is mainly to provide a plausible initial salinity stratification to start scen.#2, for which we consider a wind forcing.

Scen.#3 considers sediment transport and takes into account wind forcing starting from an initial homogeneous distribution of salinity (S=20 PSU) and a flow at rest.

For scen.#3, a thin bottom layer of mixed mud-sand sediments is considered with an initial thickness constant for the entire lagoon. The goal is to determine the temporal changes of this thickness as well as the changes in sediment composition induced bythe currents generated by a strong wind. This scenario is discussed in Section 5.1.

3.5. Seawater inflow

The Caronte channel by which the Mediterranean seawater penetrates into the lagoon is narrow (100-250 m wide) and long (6.5 km). From our previous studies (Alekseeko et al., 2013a,b), we expect that the tidal contribution of the seawater inflow does not create a substantial current in the nearshore replanting zones. So, the sea tide, semi-diurnal, is still simply represented by a harmonic law for the surface elevation at the open boundary of the Caronte channel:

$$\eta(t) = 0.3 \cos\left(2\pi(t - t_0)/T\right), \tag{6}$$

where t_0 denotes the initial time of computation, T is the tidal period (about 44714 s or 12h25 min). The tidal amplitude of 0.3 m was chosen corresponding to local tide-gauge measurements in the Golf of Fos at the entrance of the Caronte channel. It corresponds to a maximum amplitude (see REFMAR (2015).

The sea salinity at the entrance of the Caronte channel is of 38 PSU, according to the salinity measurements in Caronte channel (at the surface and at the bottom) shown in the Fig.14 of the report by SOGREAH (2009).

3.6. Freshwater inflow

Hydropower runoff is fixed at its weekly average value, i.e., 80 m^3/s. The two rivers, Arc and Touloubre, are considered with the mean runoffs of 5 m^3/s and 3 m^3/s, respectively.

4. Wind effect on *BSS* for various wind directions; weighted average effect

The present section is aimed to extend the previous numerical study (Alekseenko et al. 2017) in the case of different wind directions, and a moderate hydropower runoff of 80 m^3/s.

The weather database (Average daily wind speed at 10 m) provided by SOGREAH (2003) for the ten-years period 1992-2001 will be used (Fig.2). It gives the mean annual frequency of wind speeds of 21 m/s and 11 m/s, in 16 directions. The dominant winds direction is N-NW, and the wind speed exceeds 11 m/s for over 102 days per year (Alekseenko et al, 2017, see their Table 2).

The numerical simulation has been organized in the way described in Section 3.5, for a wind speed of 21 m/s. First, the calculations are performed for the scen.#1 for 14 days, with the initial salinity S=20 PSU, and a sea salinity at the entrance of Caronte channel of 38 PSU. Concerning the bottom drag coefficient, the bottom roughness parameter z_0=0.0001 m has been used in eq.(3). It would correspond, according to Dufois & Le Hir (2015), to a particle diameter of d=1200 μm (coarse sand).

Then, the time evolution of the 3D hydrodynamics has been calculated for the scen.#2 starting from the stratified field at the end of scen.#1. The same simulation strategy has been realized for each of the 16 wind directions of the wind rose. Concerning the surface drag, in eq.(1), the value of $Cd_s = 0.0032$ given by Young (1999) has been used for the wind speed of 21 m/s.

The presentation of the results is limited to the bottom shear stress (*BSS*) which is defined by $BSS = \sqrt{\tau_{b,x}^2 + \tau_{b,y}^2}$. The *BSS* maps for six directions, around the two main directions: N-NW and S-SE are given in Fig.3. These maps are very similar. They all indicate the presence of downwind coastal jets along the eastern and western shores. In such a semi-enclosed lagoon, the hydrodynamics is characterized by a windward surface current, a downwelling at the opposite shore and return flow occurring over the deeper regions (Csanady,

1971). For the wind directions of the N-NW sector, this downwelling mechanism increases BSS along the Southern shore. Reversely, for the wind directions of the S-SE sector, the downwelling mechanism increases BSS along the Northern shore (Fig.3).

Then we tried to determine if some additive effect of all these wind contributions could generate a larger effect on BSS or not, compared to the N-NW wind. For that purpose, a weighted summing of the BSS values of each of the 16 wind directions has been realized by using the frequency of wind occurrence in each direction, given in Fig.2. The corresponding 2D maps for the entire EB lagoon are given in Figs.4a and 4b. These two figures give the possibility, by comparing BSS to BSS_{cr} for different particle diameters, to give a rough estimation of the places in EB lagoon where the risk of erosion is higher. It is not in the scope of the present paper to determine the exact place where the erosion risk is higher. Our Figs.4a and 4b already indicate that the risk exists in several coastal areas. To determine more exactly the places of higher risk, it would be needed to measure the bottom sediment properties in the relevant places and, then, to repeat the numerical experiments with these more accurate properties.

Then, by summing the effect of the different wind directions on the two BSS components ($\tau_{b,x}$, $\tau_{b,y}$), we can get the mean direction of the bottom current (Figs.4c and 4d), and we can expect that it will indicate the preferable direction for the Z.n. propagation (dynamic resilience) year after year.

5. Transport of bottom sediments: erosion and burial

The sediment transport is often a stressor for SAV restoration or resilience. According to Cabaco & Santos (2007) and Han et al., (2012) the critical level of burial or erosion tolerated by Z.n. is extremely low (between 4 and 8 cm) due to the small size of the species and the lack of vertical rhizomes.

In the present work, a thin bottom layer of mixed mud-sand sediments is considered with an initial thickness constant for the entire lagoon. The goal is to determine the temporal changes of this thickness as well as the changes in sediment composition induced by the currents generated by a strong wind.

5.1. Model description

In this part, we use the sediment transport model SEDIM described in Section 3.4. The choice of particles has been inspired by the experimental data of Rigaud (2011), mentioned above, concerning mud-sand sediment in two deep places in EB. We consider an initial sediment composition with 25 % of fine sand of 160μm, 25% of very fine sand of 80μm, 25% of coarse silt of 40μm and 25% of medium silt of 20μm (Table 1).

SEDIM model involves a space filling procedure described by Le Hir et al (2011) and clearly illustrated on their Figs.4a-b. This space filling procedure to obtain mixed mud-sand sediment is applied to an initial sediment column of thickness 120cm. Typical ranges of porosity (void fraction - a percentage between 0 and 100%) have to be respected whatever the combination of particle types. We took a porosity equal to 0.45 for pure sand and of 0.55 for mixed silt/sand (Hopmans & Rolson, 2000, see their Table 2.6). At the beginning of simulation, we use 5 sediment sublayers containing four particle types in equal concentration (100 kg/m³).

After the space filling procedure, the thickness of the mixed sediment column is reduced to 15 cm, and the concentration of each particle type in each sublayer reaches 200 kg/m³. The thickness of each sublayer of mixed sediment became equal to 3 cm.

SEDIM model involves a sedimentation process, for which we need to provide settling velocity W_s of the different suspended sediments and critical shear stress of deposition which,

following Winterwerp (2007), is taken as BSS_{cr} (Table 1). For the two cohesive substances (silts), the settling velocity is considered to be constant (i.e. we do not take into account a flocculation process) and has been estimated using the Stokes law. For non-cohesive particles (sands), the settling velocity is taken from Soulsby formulation (after Le Hir et al.,2011 or Dufois & Le Hir, 2015).

For the deposition process, when all 5 sublayers are filled up, SEDIM model provides 5 additional sublayers to be filled.

The bottom roughness z_0 which appears in eq.3 is assumed to only depend on the sediment size. After Dufois & Le Hir (2015), the following relationship is used: $z_0=2.5d/30$ where d is the particle diameter. The diameter of the coarser modeled particle – fine sand (160μm) – has been chosen; leading to $z_0=13.3$μm. Concerning the erosion rate E_0 needed to calculate the erosion fluxes, most of the calculations have been performed for $E_0=0.001$ kg/m^2/s. According to the experimental data provided by Amos et al. (2010) for a semi-enclosed lagoon (Venice), this value corresponds to a maximum effect on the erosion flux. The influence of this important parameter is analyzed in Subsection 5.6.

5.2. Erosion and redeposition results for a N-NW wind of 21 m/s

Fig.5 shows the time-evolution, every 6h, of sediment thickness for the N-NW wind of 21 m/s. To better identify the zones of erosion and deposition, we present the thickness relative to the initial level (0 m – at the sediment-water interface). The sediment is totally eroded when the thickness reaches -15 cm. Reversely, when the relative thickness is positive, it corresponds to deposition. The sediment is rapidly eroded on eastern nearshore of EB and in the Etang de Vaine. In these zones, almost all sands and silts have disappeared after the first 24 h. Eroded and deposition zones enlarge with time. In most of the central part of EB, the initial thickness increases in the range of 3-6 cm, but in the Etang de Vaine it increases up to 10 cm. So, according to the criteria given by Cabaço & Santos (2007), there is a risk of burial in the Etang de Vaine. Deposition zones could be seen also as zones which stock not only the eroded sediments but also Z.n. spores settling for the next reproduction.

Fig. 6a shows the time-evolution of sediment thickness at the four nearshore control places (PA, PB, PF and PM; initially selected for Z.n. replanting). For this wind of 21 m/s, the initial sediment layer of 15 cm is totally eroded during the 40 hours. Erosion is faster at PA and PM: the erodible sediment thickness is reduced to almost zero after the first 4 and 10 hours, respectively. At PF, remarkably, sediment thickness slightly re-increases of 1-2 cm, cyclically, at the hours 42, 54 and 66. This can be related to the sea tide influence since this point is closer to the sea, and deeper than the others. Figs. 6a also show the time evolution of the sediment thickness at PBd, PAd and PVd, inside the deposition zones exhibited in Fig.5. These points are selected near PB, PA and PV, respectively. The maximal sediment accumulation is found at PVd where the increase of sediment thickness became larger than 15 cm.

This thickness evolution with time is particularly well correlated with the silt fraction changes shown in Figs.6b-h. Silt fraction increases in all deposition points and decreases in all erosion points; this could be related to the fact that silt is firstly resuspended in the high energy currents due to its low BSS_{cr}. Sand fraction increases in the nearshore control points while sediment thickness decreases; inducing an increase of sand concentration. Such a behavior of very high concentration vs very small residual sediment is mentioned by Le Hir et al. (2011); they call it as a fast segregation of sand (see, their Fig.7c). The nearshore control points selected for the replanting program are vulnerable for erosion and have tendency to contain more sands than silts in their sediment substrates, while the other points, where deposition mainly occurs, should contain more silts.

Erosion risk in EB is simply determined by comparing BSS with the critical value,

BSS_{cr}, at which the sediment mobility occurs as a function of particle sizes. Due to the lack of available data about cohesiveness of EB sediments, BSS_{cr} has been evaluated according to the work of Berenbrock & Tranmer (2008) which follows the classical Shields approach for cohesionless sediment. For the four sediment types used in our model, BSS_{cr} varies in the range of 0.070 - 0.160 N/m^2.

In Figs.7, we construct BSS classification maps (in N/m^2) for each sediment class based on their corresponding values of BSS_{cr} (Table 1). These maps are useful to analyze areas subjected to different types of erosion (floc, surface and mass erosion) defined in Section 3.4. White areas correspond to the places without erosion ($BSS < 0.5BSS_{cr}$). Most wide areas are impacted by floc erosion ($0.5BSS_{cr} < BSS < 1.5BSS_{cr}$; resuspention of individual particles of the surficial sediment layer). Surface erosion ($1.5BSS_{cr} < BSS < 3BSS_{cr}$), appears in the central part for both types of sand, and in the northern part of EB for the very fine sand (Figs.7a,b). For silts (Figs.7c,d), these two areas are connecting and creating a pattern all along the central part of EB - from North to South. Surface erosion area is the largest for the smallest sediment class: medium silt (Fig.7d).

Mass erosion ($BSS > 3BSS_{cr}$) occurs for all sediment classes along most of the coastal zones. In addition, it occurs in the central part of EB, except for fine sand. Mass erosion areas enlarge when the grain size decreases. Mass erosion mostly impacts the smallest particles.

5.3. Erosion risk for different winds

We first analyze how BSS maps depend on the wind speeds (21, 11, and 6 m/s) of the N-NW wind after 3 days (Figs.8). The goal is to evaluate erosion risk; i.e., the areas where BSS exceeds BSS_{cr} of each of the four particle types (Table 1). As it was expected, the stronger wind induces higher BSS in the entire EB; highest BSS is observed along the eastern shore. Along the eastern coastal zone, sediment bed could be strongly eroded, since their BSS (yellow and orange colors) largely exceed BSS_{cr} (Figs.8a).

Fig.8c shows that even for N-NW wind of 6 m/s, BSS reaches 0.1 N/m^2 (green colors) which is larger than BSS_{cr} for silt in different places. It occurs in particular in mouth of Arc River, Etang de Vaine, near the entrance of the Caronte channel and inside this channel. So, sediment mobility and resuspension of fine sediments (silts) into water column could occur in these places (which are indicated in Fig.1).

For moderate N-NW wind of 11 m/s, silt erosion (green colors) could occur in the major part of EB coastal zone (Fig.8b). Some areas represented by magenta and blue colors would be not subject to erosion (their BSS being lower than BSS_{cr}); so, these areas could be favorable for Z.n. resilience. For a stronger N-NW wind of 21 m/s, these areas reduce their surface, but still exist (Fig.8a).

It is also interesting to analyze how the erosion risk would depend on wind direction. So, two wind speeds (21 m/s and 11 m/s) in S-SE direction have been selected, for the same initial sediment thickness of 15 cm. BSS maps (Figs.9a-b) reveal a risk of erosion over the eastern and western shores, and in some zones of the northern part of EB, marked by red colors. In addition, thickness maps (Figs.9c-d) show that the highest erosion is obtained in areas where BSS exceeds 1 N/m^2 for the wind speed of 21 m/s, and 0.1 N/m^2 for the wind speed of 11 m/s.

This erosion risk along eastern shore in EB is more important than for wind of N-NW direction at the same wind speed of 21 m/s. This tendency is confirmed in Figs.10 by comparing the time-evolution of the sediment thickness. Erosion at the two eastern sites (PA and PB) is much larger for the S-SE wind; 15 cm are eroded at PA after 3 h and at PB after 8 h. For the two western sites (PM and PF), the behavior is different: the initial sediment thickness of 15 cm is totally eroded at PM after 28 h, while it increases at PF up to 30 cm due to redeposition process.

Concerning the three deposition points selected for N-NW wind, the initial sediment thickness of 15 cm is eroded at PAd during the first 12 h, while in PVd and PBd the sediment thickness increases (Fig.10d). This means that at least for these two points, N-NW and S-SE winds contribute to increase deposition. On the contrary, a different behavior between S-SE and N-NW winds is found in PF (Fig.10a) and in PAd (Fig.10b). But this is without consequence for our analysis for erosion and burial risks.

For wind speed of 11 m/s, the time evolution of the sediment thickness is compared at the four control places for the two opposite directions N-NW (Fig.11a) and S-SE (Fig.11b). At PA, erosion is very fast for both wind directions. It is faster for S-SE wind (less frequent). At PB, the erosion appears also to be faster for S-SE wind. At PF, like in the case of larger wind speed, there is a deposition for S-SE wind, instead of erosion for N-NW wind. But, the way in which the comparison is made (only at four points) presents some drawback.

A global comparison between Figs.8a and 9a for the wind of 21 m/s, and Figs.8b and 9b for the wind of 11 m/s, show that both wind directions give an additive contribution on *BSS* and would lead to the same conclusion about additive effect on erosion at least along the eastern and western shores.

It is interesting to point out that Paquier et al. (2014) presented seasonal bathymetric and beach topographic in a small shallow bay very close to PB in EB. The beach is subject, alternatively, to sedimentation and erosion, with changes attaining up to about 0.5m over a period of several months. Such large changes can be due not only to the bottom current generated by the strong winds during such a long period, but also by the wave dynamics which are not yet taken into account in our model.

5.4. Sensibility tests

As the exact characteristics of bottom sediments, such as grain-size proportion and erosion rate, are not yet available, and anyway are not constant in all EB, additional numerical experiments are performed to evaluate the impact of such uncertainty on the prediction of sediment thickness. Two tests have been performed for N-NW wind of 21 m/s. Two additional compositions have been tested (see Table 2). One with 90% of mud and 10% sand, called DF (deep fraction) which imitates the sedimentary layer in deep part of EB, and another one, called CF (coastal fraction), which is supposed to better represent coastal sediments with 50% of mud and 50% of sand.

Figs.12a show the time evolution of sediment thickness at PB and PA identified as erosion sites. At PA, the erosion is rapid: 4 hours for DF composition and 8 hours for CF composition. This is related to the fact that DF composition contains more mud which is rapidly suspended due to its lower BSS_{cr}. At PB, the initial sedimentary layer is totally eroded for DF composition during the first 16h; while for CF composition the full erosion requires 72 hours.

Figs.12b show the time evolution of sediment thickness at PBd and PAd identified as redeposition sites. The redeposition is higher for DF composition which contains more silt. This is expected since the erosion was larger in this case.

Solid red curves representing CF composition in Figs.12a-b for erosion points PB, PA could be compared to the curves plotted in Fig.6a for the corresponding points, where the erosion was more rapid. This faster erosion can be explained by the fact that CF composition corresponds to a larger amount of sand of larger size (50% of sand of size of 200μm) than in the case of Fig.6a (50% of sands of sizes of 80μm and 160μm, in equal proportion).

For the CF composition, we check the effect of erosion rate E_0 (second sensibility test), in the range of 10^{-4} to 10^{-3} kg/m²/s inspired by the work of Amos et al. (2010) for Venetian lagoons (Figs.13).

The time evolution of the sediment thickness vs E_0 is presented at the four nearshore

control points subjected to erosion in EB (Figs.13a-d). As it was expected, erosion is less pronounced for lower E_0. For $E_0 = 10^{-3}$ kg/m^2/s: the initial sedimentary layer of 15 cm was totally eroded after 72 hours in all the control points (PA, PB, PF and PM).

For E_0 ten times lower, after 72 hours, the initial sediment layer is totally eroded only at PA. At the other erosion points, the erosion process is strongly decelerated: the decrease of sediment thickness is only of 1.5 cm at PB, and of 3 cm at PF.

The time evolution of the sediment thickness vs E_0 is also presented for the three deposition points PVd, PBd and PAd (Figs.13e-g). Sediment thickness is increasing only in the range of 0.5 - 1.5 cm during 72 hours (Figs.13e-g). It is to remark that for the conditions discussed in this subsection, contrary to those used for Fig.6a, the increases of bottom sediment thickness never reaches the critical level of deposition.

6. Discussion and conclusion

In Section 4, the *BSS* maps have been determined for the 16 directions (given from a wind rose) of a wind speed of 21 m/s, in order to analyze the potential additional effect of these winds on the SAV roots, a mean value of |*BSS*|. A weighted average based on the frequency of each wind directions, has been determined and compared to BSS_{cr} corresponding to a class of roughness parameters. In addition, an averaging of the two components of *BSS* has been evaluated, similarly, in order to obtain the direction of an average bottom current which could be compared with the preferential direction of propagation of resilient Z.n. observed year after year (Bazile, 2017).

In Section 5, we have analyzed how the thickness of a given layer of mud-sand bottom sediments is changed (resuspension and/or redeposition) due to wind effect in EB, for the two main wind directions (N-NW and S-SE) and for three wind speeds. Although bottom sediments in EB contain a large fraction of mud, their cohesiveness is not considered in the present work due to a lack of specific experimental data. The present modelling of sedimentary dynamics take mainly into account theoretical thresholds for sand and for mud, and surficial erosion flux which is proportional to an erosion rate. For this erosion rate, we used values in the range 10^{-4} to 10^{-3} kg/m^2/s determined experimentally for the Venetian ones which have similar sediment composition.

The time evolution of the initial sedimentary layer, for a period of 3 days, permits to determine the area where the erosion would be large enough in EB to be a stressor for the SAV restoration (resilience or replanting). The main results are presented as *BSS* maps for the entire EB. Then, time evolution of sediment thickness is presented at 4 places subjected mainly to erosion (PA and PB, on the eastern shore) and (PM and PF, on the western shore). It is also presented in three places subjected mainly to deposition (PAd and PBd, near PA and PB in EB) and PVd (in Etang de Vaïne).

Erosion is maximum in the areas where *BSS* is maximum (e.g., at PA and PB) due to the coastal jets. It is larger for the S-SE wind of the same speed (but less frequent). Deposition is found in the nearshore areas where *BSS* is close to zero due to coastal jets. The time evolution of the sedimentary thickness given in Fig.5 permits to determine when and where the risk to overpass the critical levels of erosion and burial tolerated by Z.n. has to be expected. For an extreme erosion rate of 10^{-3} kg/m^2/s and a strong wind speed of 21 m/s, all the initial sediment layer of 15cm would be eroded in several nearshore areas. The erosion risk is maximum along the eastern shore, where an additive effect of the two opposite winds can be expected. Indeed, S-SE and N-NW winds create coastal jets of opposite direction and of about the same intensity (for the same speed) exerting alongshore erosion and deposition at about the same places.

BSS classification maps have been presented in Fig.7 for the 3 types of erosion (floc, surface and mass) described by several authors.

In Figs.13, the temporal evolution of the sediment thickness for a lower erosion rate of 10^{-4} kg/m²/s shows that, even in this case, the risk of an erosion overpassing the limit for Z.n. survival (between 4 and 8 cm; according to Cabaco & Santos 2007) would have to be expected in some places.

Of course, the accuracy of the present model to determine erosion and deposition is limited by the lack of adequacy of the input data that would be needed to calibrate it. In particular, the expression of BSS_{cr} is limited to a cohesiveless sediment. The present results concerning the time evolution of erosion depth induced by the wind improve our knowledge of the erosion risk on the Z.n. restoration in EB. They will be useful to appropriately orient the action of politics and managers for a future restoration program.

Our results give insight on what future work should focus to improve our results. It will be not only needed to get reliable in situ data (at least in the possible restoration areas), but we plan also to consider in the present model the suspended matter (silts and clays involved in the hydropower inflow). In addition, we plan to take into account the effect of wave dynamics through the boundary conditions (1) and (2).

References

[1] Alekseenko E., Roux B., Sukhinov A., Kotarba R., Fougere D., 2013a. Coastal hydrodynamics in a windy lagoon. Computers & Fluids 77, 24–35.

[2] Alekseenko, E., Roux, B., Sukhinov, a., Kotarba, R., Fougere, D., 2013b. Nonlinear hydrodynamics in a mediterranean lagoon. Nonlinear Processes in Geophysics, 20(2), 189 198, 2013. http ://doi.org/10.5194/npg-20-189-2013.

[3] Alekseenko E., Roux B., Fougere D., Chen P.G., 2017. Coastal hydrodynamics in a windy lagoon. Estuarine, Coastal and Shelf Science 73 :617–629.

[4] Alekseenko E., Roux B., 2017. Numerical simulation of the wind influence on bottom shear stress and salinity fields in areas of Zostera noltei replanting in a Mediterranean coastal lagoon. Progress in Oceanography, *https : //doi.org/*10.1016*/j.pocean.*2017.05.001.

[5] Amos C.L., Umgiesser G., Ferrarin C., Thompson C.E.L., Whitehouse R.J.S., Sutherland T.F., Bergamasco A. 2010. The erosion rates of cohesive sediments in Venice lagoon. Continental Shelf Research, 30 (2010) 859-870.

[6] Bazile P., 2015. Le rapide développement des herbiers de zostères de l'étang de Berre. 27 mai 2015. *https : //letangnouveau.wordpress.com/*2015/05/27/le − rapide − developpement−des−herbiers−de−zosteres−de−letang−de−berre/.

[7] Bazile P., 2017. 1ère campagne de Survey des zostères de l'étang de Berre par drone (9-10 juillet 2017). *http ://letangnouveau.wordpress.com/*2017/07/09/survey − zosteres −drone − no1/.

[8] Berenbrock C. and Tranmer A.W., 2008. Simulation of Flow, Sediment Transport, and Sediment Mobility of the Lower Coeur d'Alene River, Idaho. U.S. Environmental Protection Agency; Scientific Investigations Report 2008–5093.

[9] Berlamont J.E. and Torfs H.M., 1996. Modelling (partly) cohesive sediment transport in sewer systems. Wat. Sci. Tech. Vol. 33, No. 9, pp. 171-178.

[10] Bernard G., Boudouresque C.F. and Picon P., 2007. Long term changes in Zostera meadows in the Berre lagoon (Provence, Mediterranean Sea) ; Estuarine, Coastal and Shelf Science 73 : 617–629.

[11] Blumberg A.F. and Mellor G.L., 1986. A description of a Three- Dimensional Coastal Ocean Circulation Model, Geophysical Fluid Dynamics Program, Princeton Univ., Princeton, New Jersey, 1–16.

[12] Cayocca F., Verney R., Petton S., Caillard M., Dussauze M., Dumas F., Le Roux J.-F., Pineau L., Le Hir P., 2014. Development and validation of a sediment dynamics model within a coastal operational oceanographic system. Mercator Ocean - Quarterly Newsletter, #49-April 2014-76.

[13] Cabaço S., Santos R., 2007. Effects of burial and erosion on the seagrass Zostera noltii. J Exp Mar Biol Ecol, 340, 204-212.

[14] Chesher, T.J. & Ockenden M., 1997. Numerical modelling of mud and sand mixture. In Cohesive Sediments ; John Wiley & Sons : New York, NY, USA; pp. 395–406.

[15] Csanady G.T., 1971. Baroclinic boundary currents and long edge-waves in basins with sloping shores. J. Physical Oceanography, 1 (2) pp. 92–104.

[16] Delpy, F., Pagano, M., Blanchot, J., Carlotti, F., & Thibault- Botha, D., 2012. Man-induced hydrological changes, metazooplankton communities and invasive species in the Berre Lagoon (Mediterranean Sea, France). Marine Pollution Bulletin, 64(9), 1921–1932. http ://doi.org/10.1016/j.marpolbul.2012.06.020.

[17] Duarte C.M., Sintes T. and Marba N., 2013. Assessing the CO2 capture potential of seagrass restoration projects. Journal of Applied Ecology, 50, 1341–1349.

[18] Dufois F. and Le Hir P., 2015. Formulating Fine to Medium Sand Erosion for Suspended Sediment Transport Models. J. Mar. Sci. Eng. 3, 906-934 ; doi :10.3390/jmse3030906.

[19] Fonseca, M. S., and S. S. Bell. 1998. Influence of physical setting on seagrass landscapes near Beaufort, North Carolina, USA. Marine Ecology Progress Series 171 :109-121.

[20] Han Q., Bouma T.J., Brun F.G., Suykerbuyk W., van Katwijk M.M., 2012. Resilience of Zostera noltii to burial or erosion disturbances. Vol. 449 : 133–143, doi : 10.3354/meps09532. $http ://www.eea.europa.eu/data−and−maps/figures/ distribution−of −the − marine − angiosperm− posidonia − oceanica − and − zostera −sp − in − the −mediterranean/ #parent − fieldname − title$.

[21] Hopmans J.W. & Rolson D.E., 2000. SSC 107 – INTRODUCTORY SOIL PHYSICS, SSC107-Fall. $https : //ocw.tudelft.nl/wp −content/uploads/D.oe4625Chapter02.pdf$

[22] Koch E.W., Sanford L.P., Chen S-N, Shafer D.J., and McKee Smith J., 2006. Waves in Seagrass Systems : Review and Technical Recommendations. US Army Corps of Engineers, ERDC TR-06-15, Nov.

[23] Kombiadou, K., Ganthy, F., Verney, R., Plus, M., Sottolichio, A., 2014. Modelling the effects of Zostera noltei meadows on sediment dynamics : application to the Arcachon lagoon. Ocean Dyn. 64, 1499–1516.

[24] Lazure P. and Dumas F., 2008. An external-internal mode coupling for a 3D hydrodynamical model for applications at regional scale (MARS). Adv.Wat. Res. 31 : 233–250.

[25] Lazure P., Garnier V., Dumas F., Herry Ch., Chifflet M., 2009 Development of a hydrodynamic model of the Bay of Biscay. Validation of hydrology. Continental Shelf Research, 29(8), 985-997.

[26] Le Hir P, Cayocca F, Waeles B., 2011. Dynamics of sand and mud mixtures: a multiprocess-based modelling strategy. Cont Shelf Res 31 :S135-S149.

[27] Paquier A-E, Meule S., Anthony E.J., Bernard G., 2014. Sedimentation and erosion patterns in a low shoot-density Zostera noltii meadow in the fetch-limited Berre lagoon, Mediterranean France. Journal of Coastal Research, Special Issue No. 70, 563-567.

[28] Panagiotopoulos I., Voulgaris G., Collins, M.B., 1997. The influence of clay on the threshold of movement of fine sandy beds. Coast. Eng., 32, 19–43.

[29] REFMAR, 2015. http ://refmar.shom.fr/en/fos-sur-mer.

[30] Rigaud S., 2011. Dynamique et biodisponibilité des éléments traces métalliques dans les sédiments de l'étang de Berre. Thèse de doctorat de l'Université Aix-Marseille, june 10, 2011.

[31] SOGREAH, 2003. Berre– Etudes de premiere phase, Evaluation comparative des impacts maritimes des solutions B et T, rapport MAR/PSI-2360023 ; 28 April 2003.

[32] SOGREAH, 2009. Modelisation hydrodynamique de l'Etang de Berre et de milieux annexes, rapport -1740286 ; Fevrier 2009.

[33] Soulsby R.L., 1997. Dynamics of Marine Sands : a manual for practical applications. Thomas Telford, London, ISBN 0-7277-2584-X.

[34] Torfs H., 1994. Shape and scale effects on secondary currents and shear stress distributions in laboratory flumes. 2nd International Conference on Hydraulic Modelling, Development and Application of Physical and Mathematical Models, Stratford-upon-Avon, 14-16 June.

[35] van Rijn L.C., 2016. Critical bed-shear stress for sand-mud mixture. Note : Initiation of motion and suspension ; 1 july 2016. *http ://www.leovanrijn−sediment.com/papers/T hresholderosion*2016.*pdf*

[36] Van Ledden M., 2002. A process-based sand-mud model. Proc. Mar. Sci., 5, 577–594.

[37] Waeles B., Le Hir P., Lesueur P., Delsinne N., 2007. Modelling sand/mud
transport and morphodynamics in the Seine river mouth (France) : an attempt using a process-based approach. Hydrobiologia (2007) 588 : 69-82

[38] Warner R.F., 2012. Environmental impacts of hydroelectric power and other anthropogenic developments on the hydro morphology and ecology of the durance channel and the Etang de Berre, southeast France, J. Environmental Management 104 : 35–50.

[39] Winterwerp J.C.,2007. On the sedimentation rate of cohesive sediment. In :Maa,J.P.-Y., Sanford,L.P., Schoellhamer,D.H. (Eds.),Estuarine and Coastal Fine Sediments Dynamics, Proceedings in Marine Science,vol.8,Elsevier,pp.209–226.

[40] Williamson H. & Torfs H., 1996. Erosion of mud/sand mixtures. Coastal Engineering, 29, 1-25.

[41] Winterwerp J.C., Van Kesteren W.G.M., Van prooijen B. and Jacobs W., 2012. A conceptual framework for shear flow-induced erosion of soft cohesive sediment beds. Journal of Geophysical Research, Vol. 117, C10020.

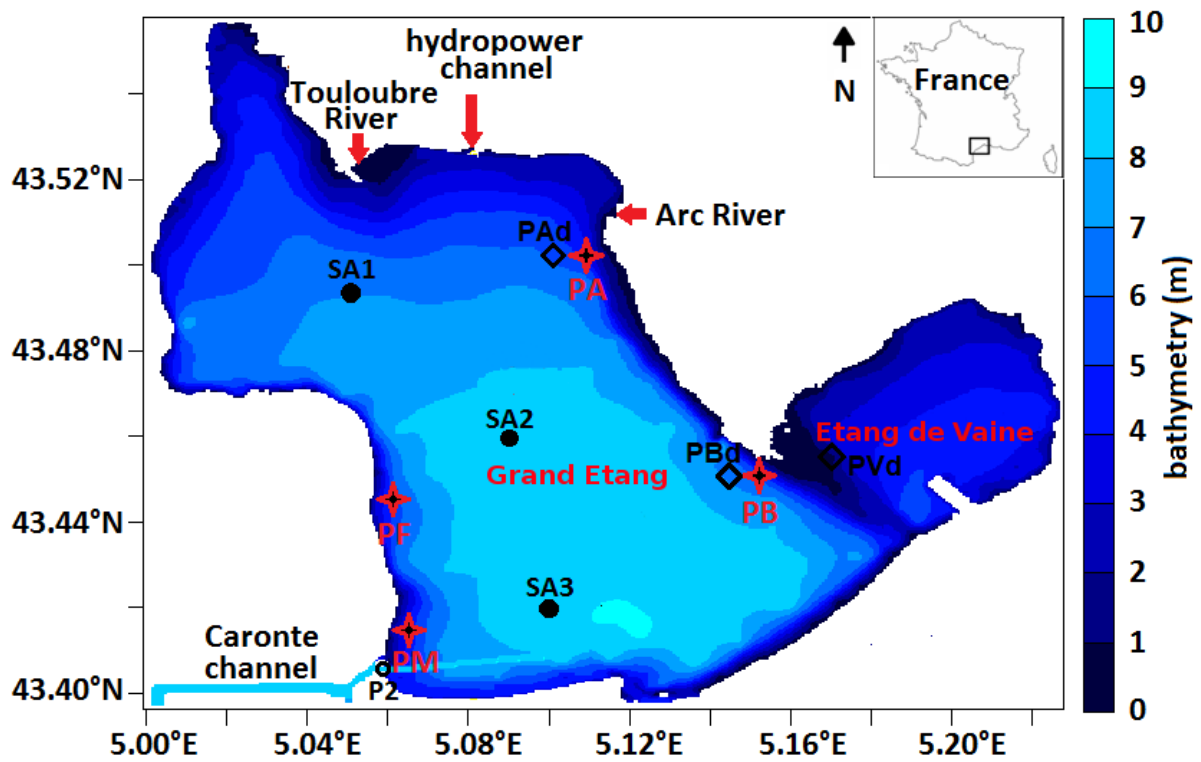[42] Young I.R., 1999. Wind Generated Ocean Waves, 288pp, Elsevier.

Fig. 1. Etang de Berre and its tributaries (hydropower channel, Touloubre and Arc Rivers), and bathymetry. Black points correspond to three mooring stations, red stars - to four nearshore control points, black diamonds - to three sediment deposit points.
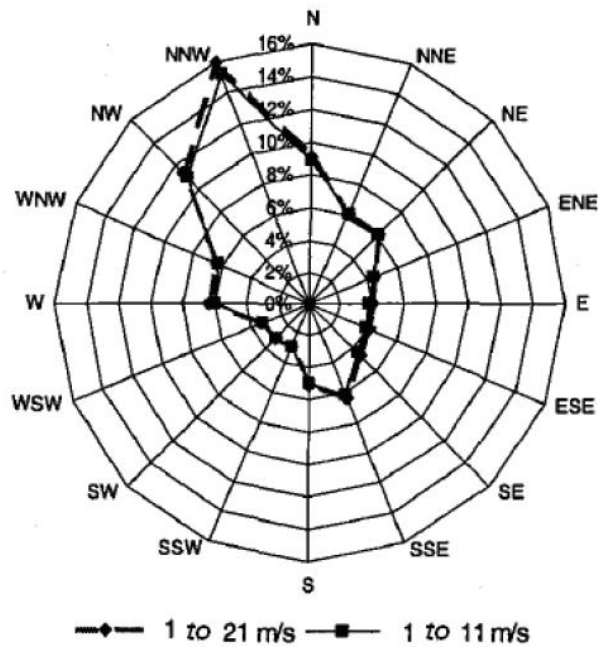

Fig. 2. Distribution of the average wind over 10 min, at the station of Port de Bouc, 10 m of height, for the period 1992–2001, 24,793 observations (Sogreah, 2003).
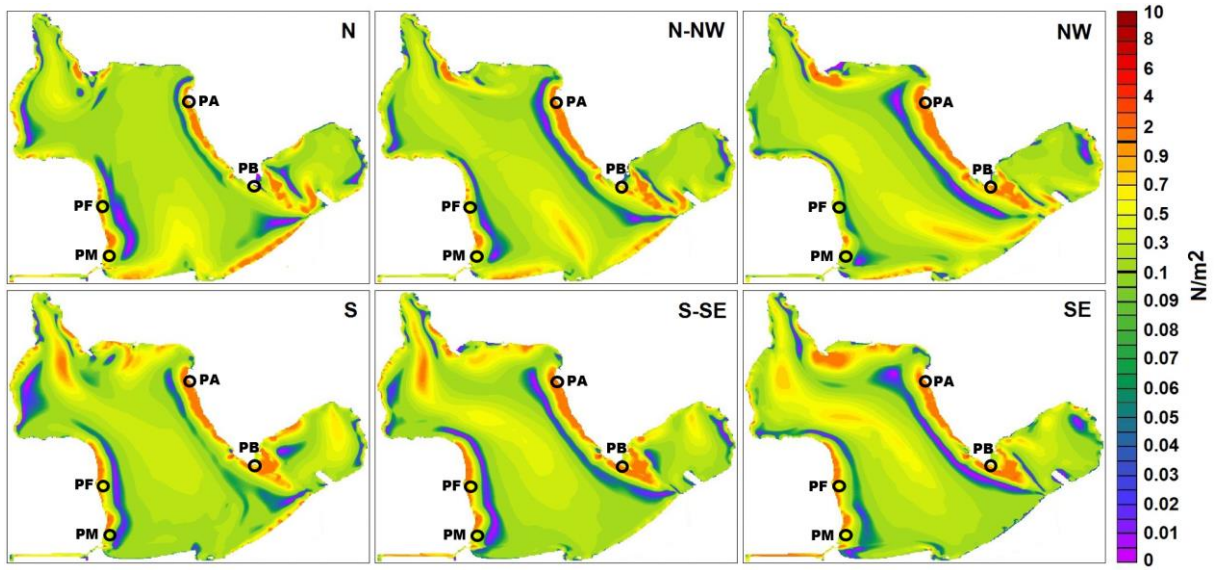
Fig. 3. Maps of BSS modulus for three wind directions in the N-NW and S-SE quadrants; for a wind speed of 21 m/s.
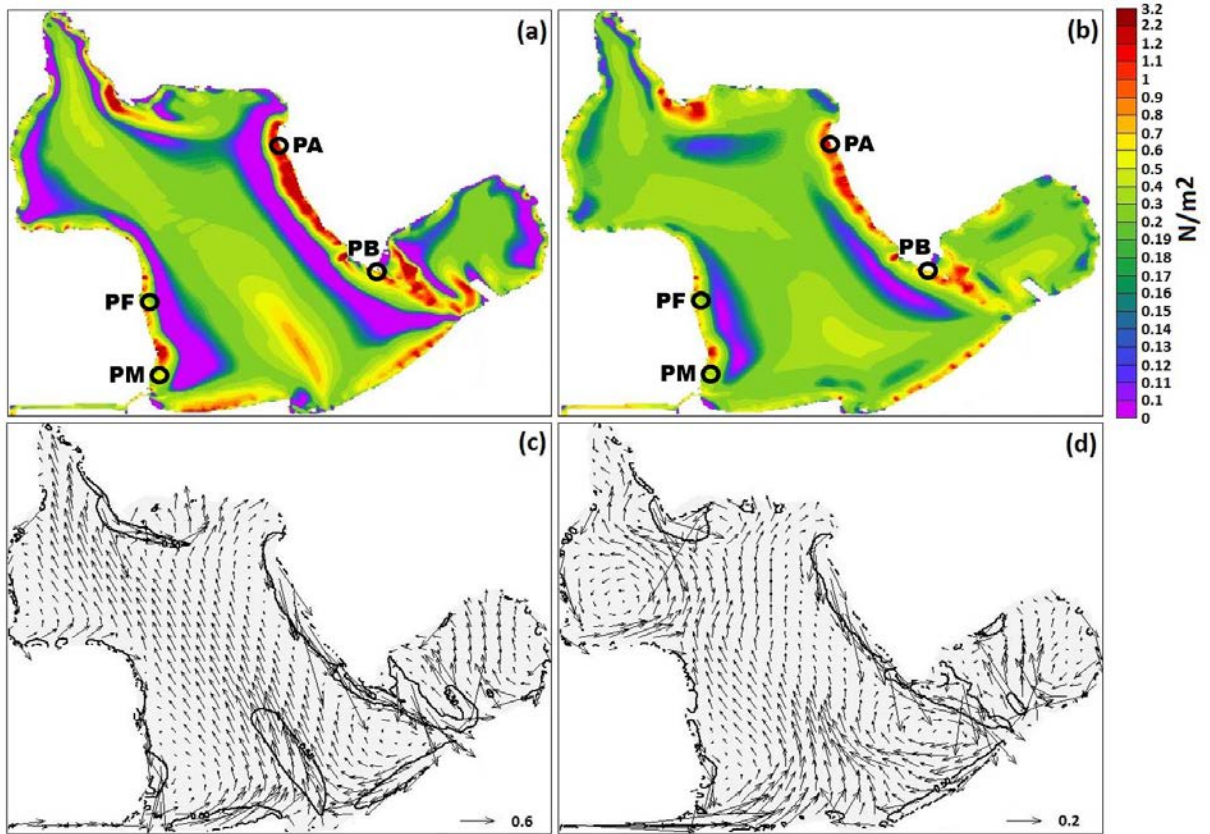
Fig. 4. BSS and vector field of the bottom stress. (a) BSS for N-NW of 21 m/s, (b) BSS for combined winds of 21 m/s, (c) bottom stress vector field for N-NW of 21 m/s, (d) bottom stress vector field for combined winds of 21 m/s. Contours on the vector field correspond to BSS = 0.5 N/m^2.
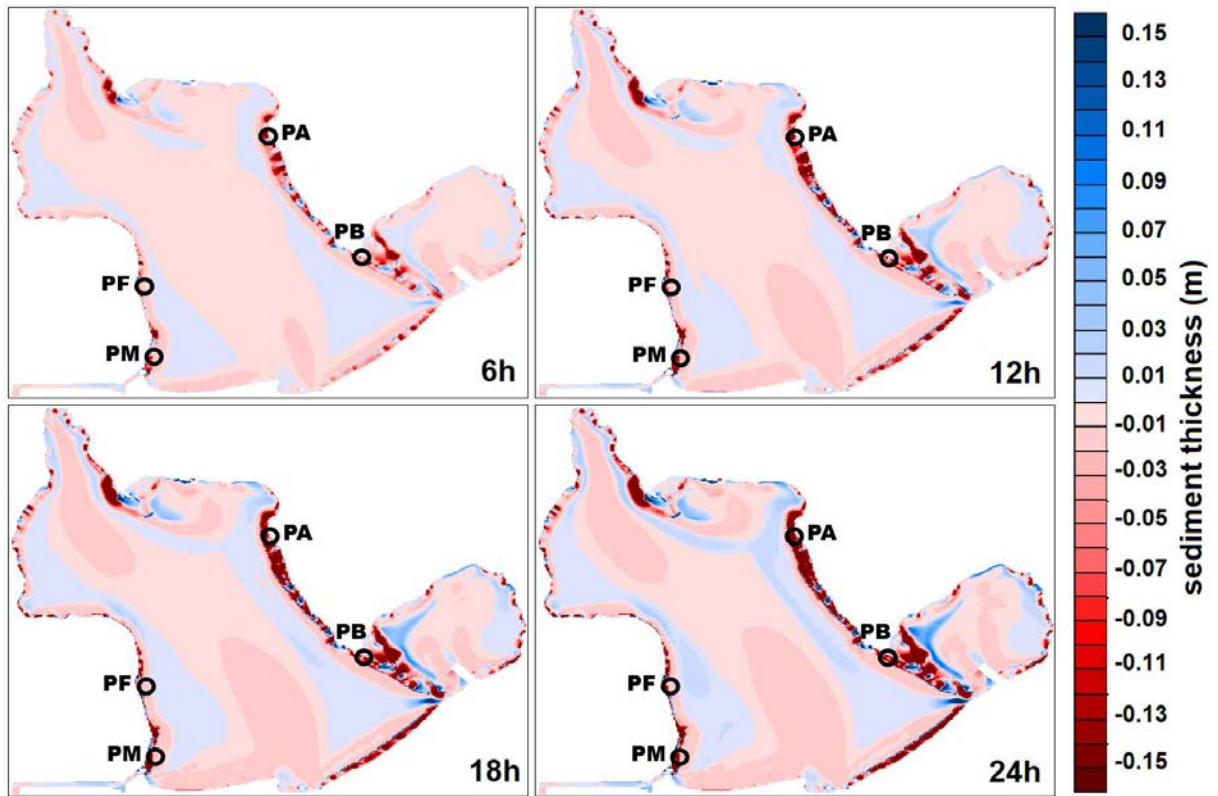
Fig. 5. Time-evolution of sediment thickness relative to the initial level (0 m – at the sediment-water interface) for N-NW of 21 m/s. Red colors correspond to erosion and blue - to deposition.
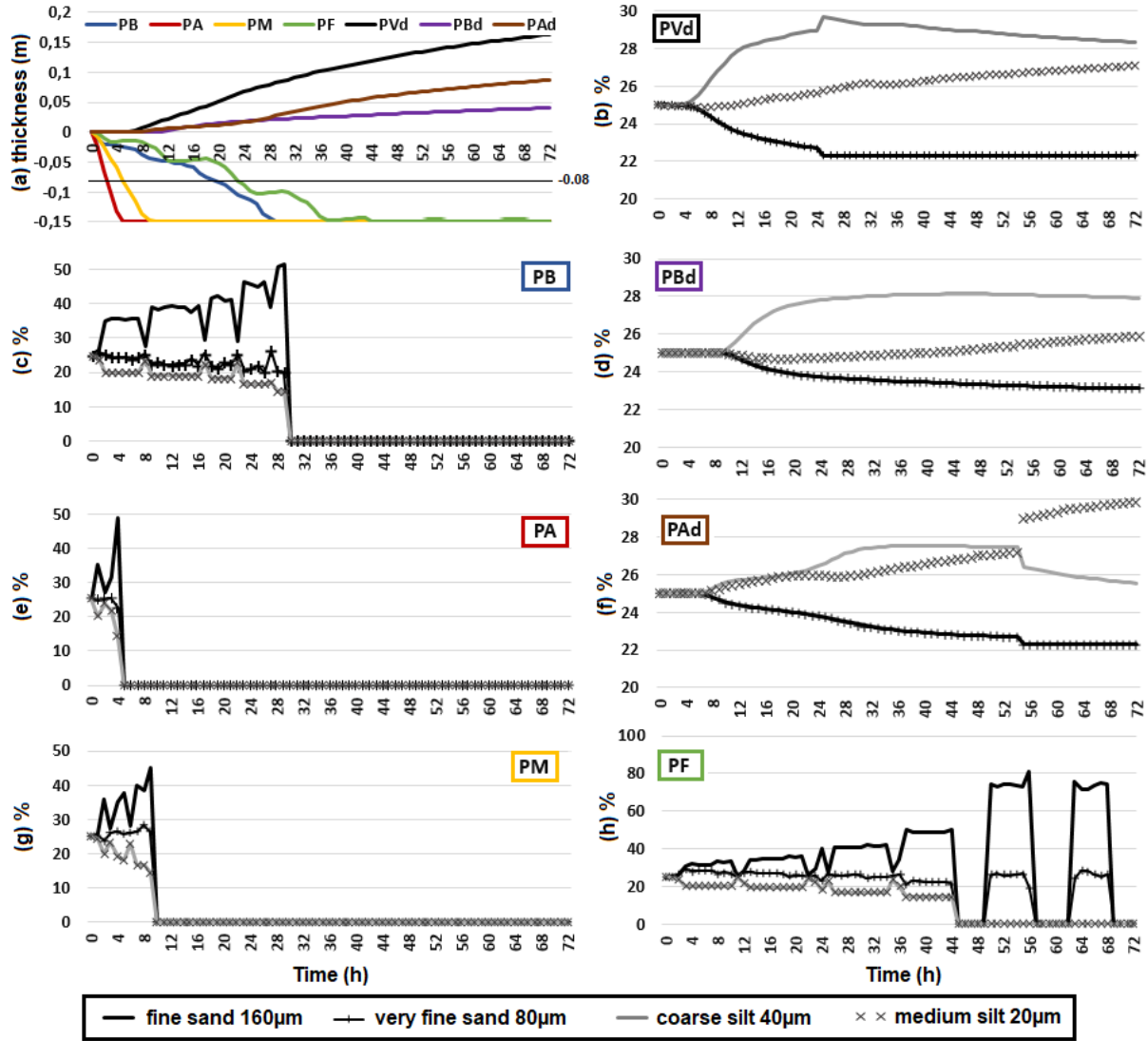
Fig. 6. Time-evolution of (a) sediment thickness (black horizontal line corresponds to the erosion limit of 8cm acceptable for Z.n. restoration); (b-h) mean fractions (over sediment column) of each class of silt and sand at PVd, PB, PBd, PA, PAd, PM and PF, respectively under a N-NW wind conditions of 21 m/s.
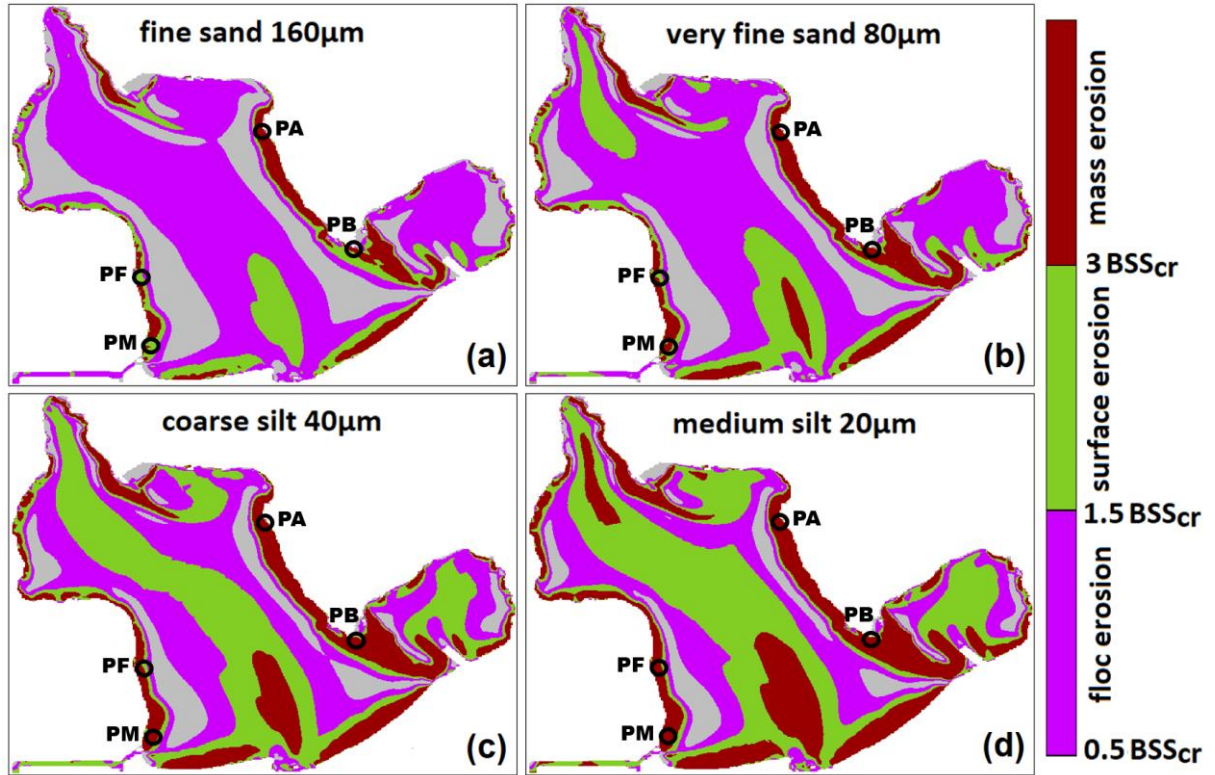
Fig. 7. BSS classification maps (in N/m^2) of three types of erosion (see definition in Section 3.4): (a) fine sand of 160 μm, (b) very fine sand of 80 μm, (c) coarse silt of 40 μm, and (d) medium silt of 20 μm. Each sediment type has its own BSS$_{cr}$ presented in the Table 1. Results were obtained for a N-NW wind of 21 m/s, after 3 days.
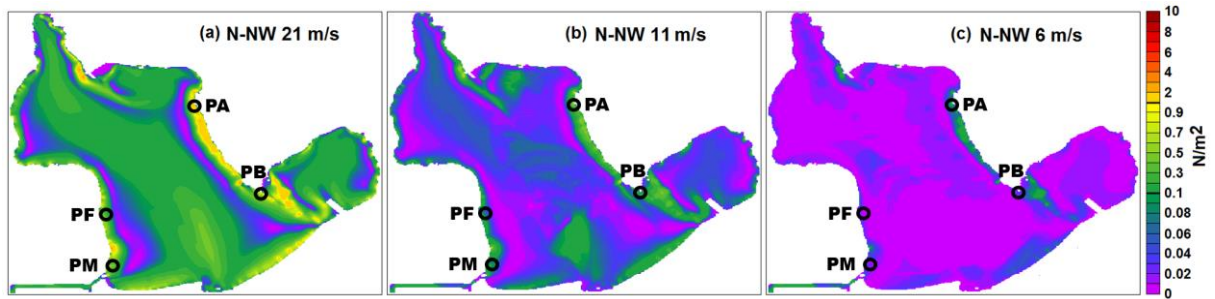
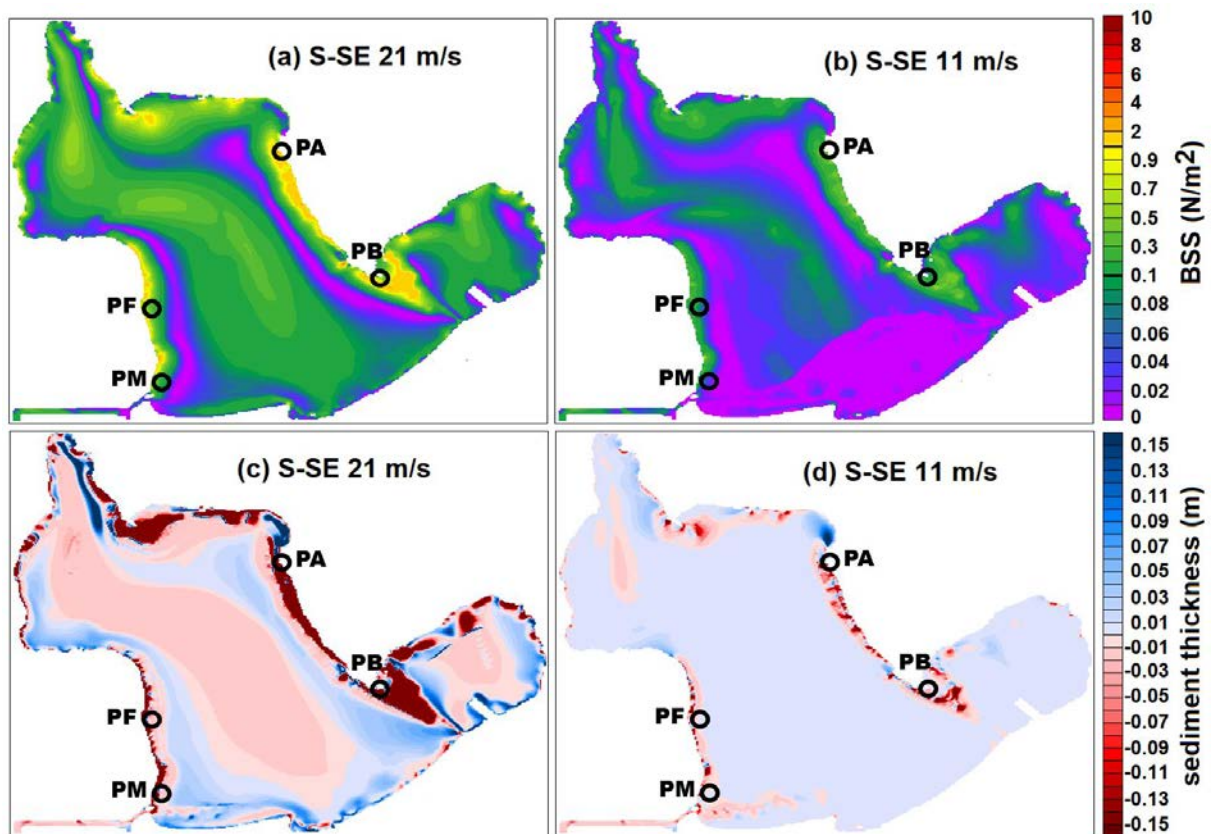Fig. 8. BSS maps for three speeds of N-NW wind after 3 days; (a) 21 m/s, (b) 11 m/s, and (c) 6 m/s.

Fig. 9. BSS after 3 days for (a) S-SE wind of 21 m/s and (b) S-SE wind of 11 m/s; sediment thickness after 3 days for (c) S-SE wind of 21 m/s and (d) S-SE wind of 11 m/s.
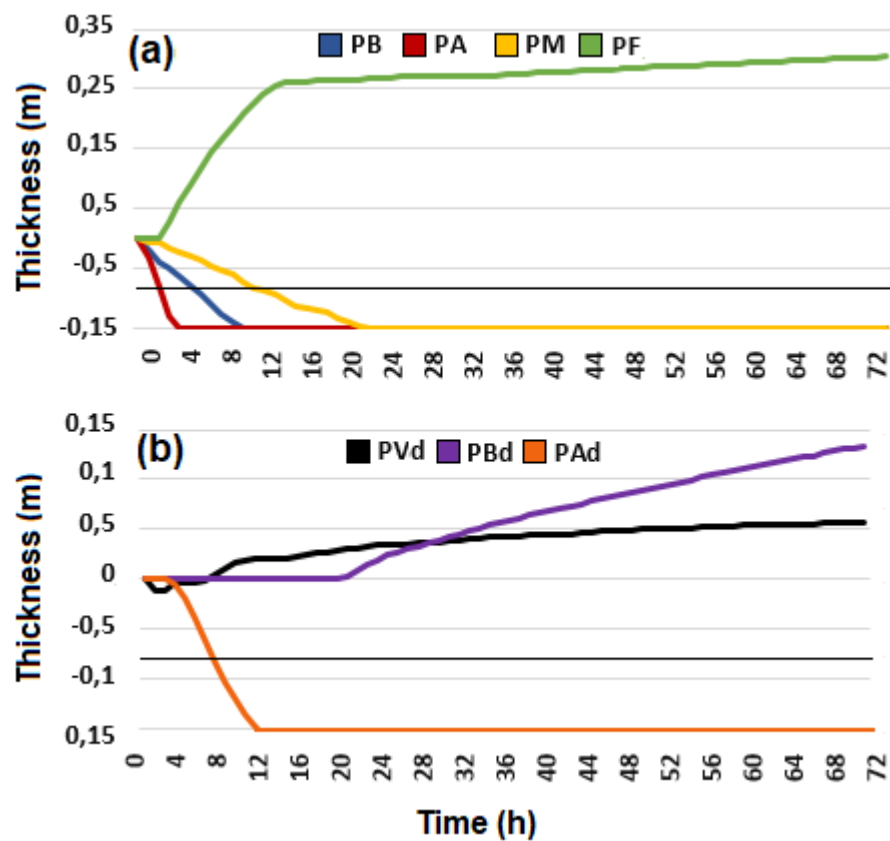
Fig. 10. Time-evolution of sediment thickness for S-SE wind of 21 m/s; (a) erosion at PB, PA, PM and PF (black horizontal line corresponds to the erosion limit of 8cm acceptable for Z.n. restoration); (b) redeposition at PVd,PBd and PAd.
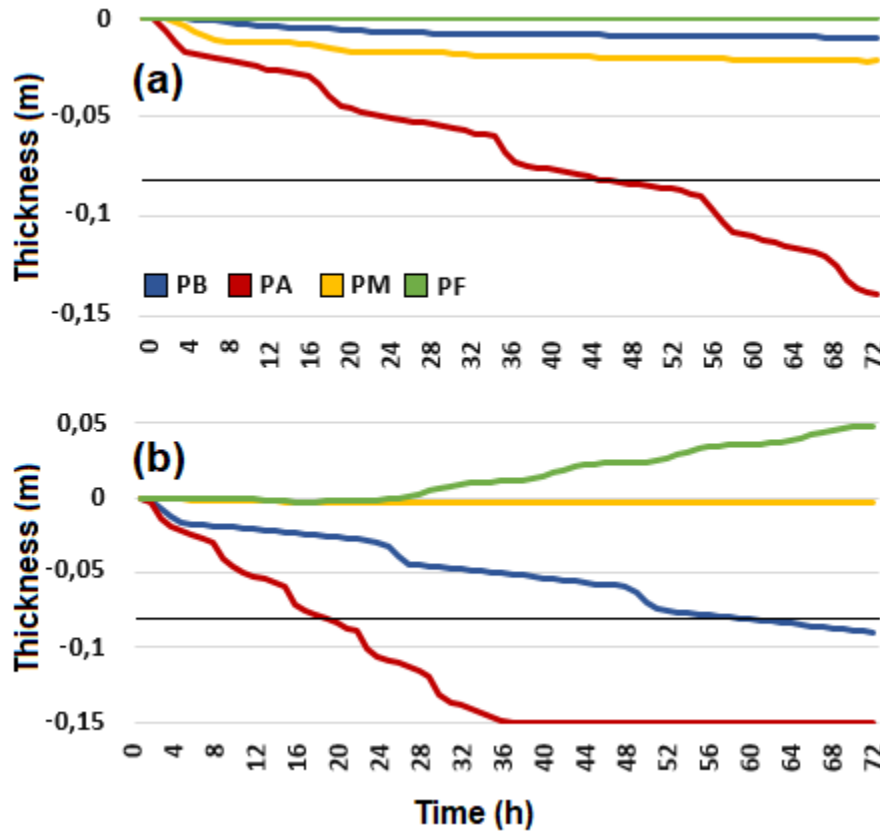
Fig. 11. Time-evolution of sediment thickness; (a) N-NW wind of 11 m/s; (b) S-SE wind of 11 m/s. Black horizontal line corresponds to the erosion limit of 8cm acceptable for Z.n. restoration.
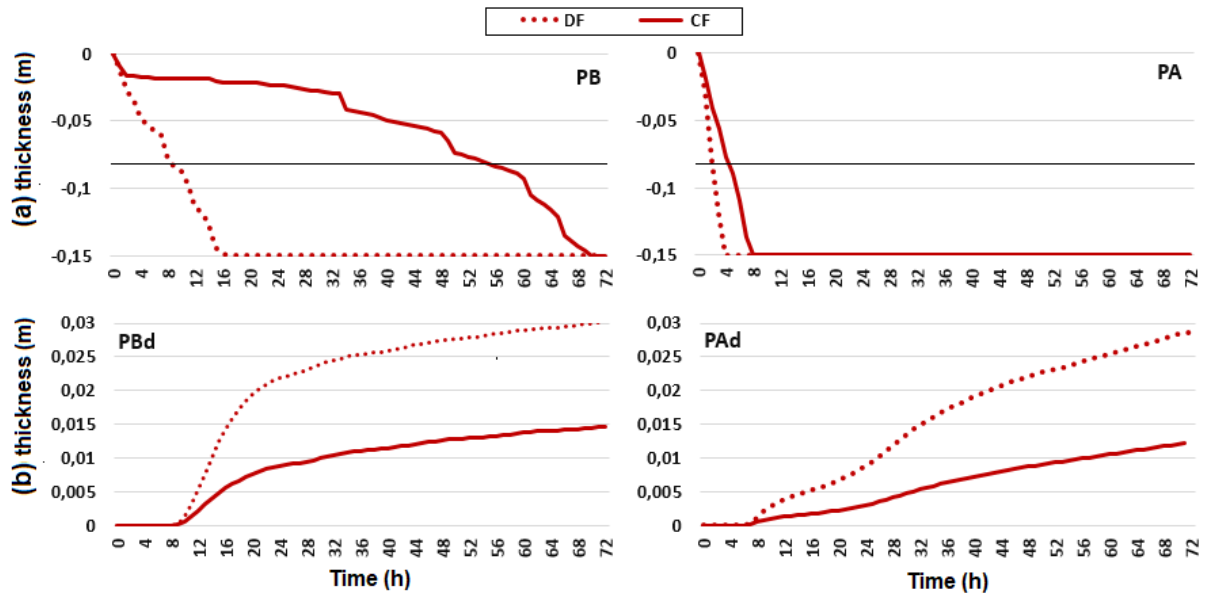
Fig. 12. Sensibility test on sediment fraction initially chosen: DF - deep fraction (90% mud – 10% sand) and CF - coastal fraction (50% mud – 50% sand), for $E_0 = 10^{-3}$ kg/m^2/s; (a) at PB

and PA subjected to erosion, (b) at PBd and PAd subjected to deposition. N-NW wind of 21 m/s. Black horizontal line corresponds to the erosion limit of 8cm acceptable for Z.n. restoration. Results corresponding to CF (solid red curves in Figs.12a) may be compared with those shown in Fig.6a for $E_0 = 10^{-3}$ kg/m^2/s and a composition (25% fine sand, 25% very fine sand, 25% coarse silt, 25% medium silt).
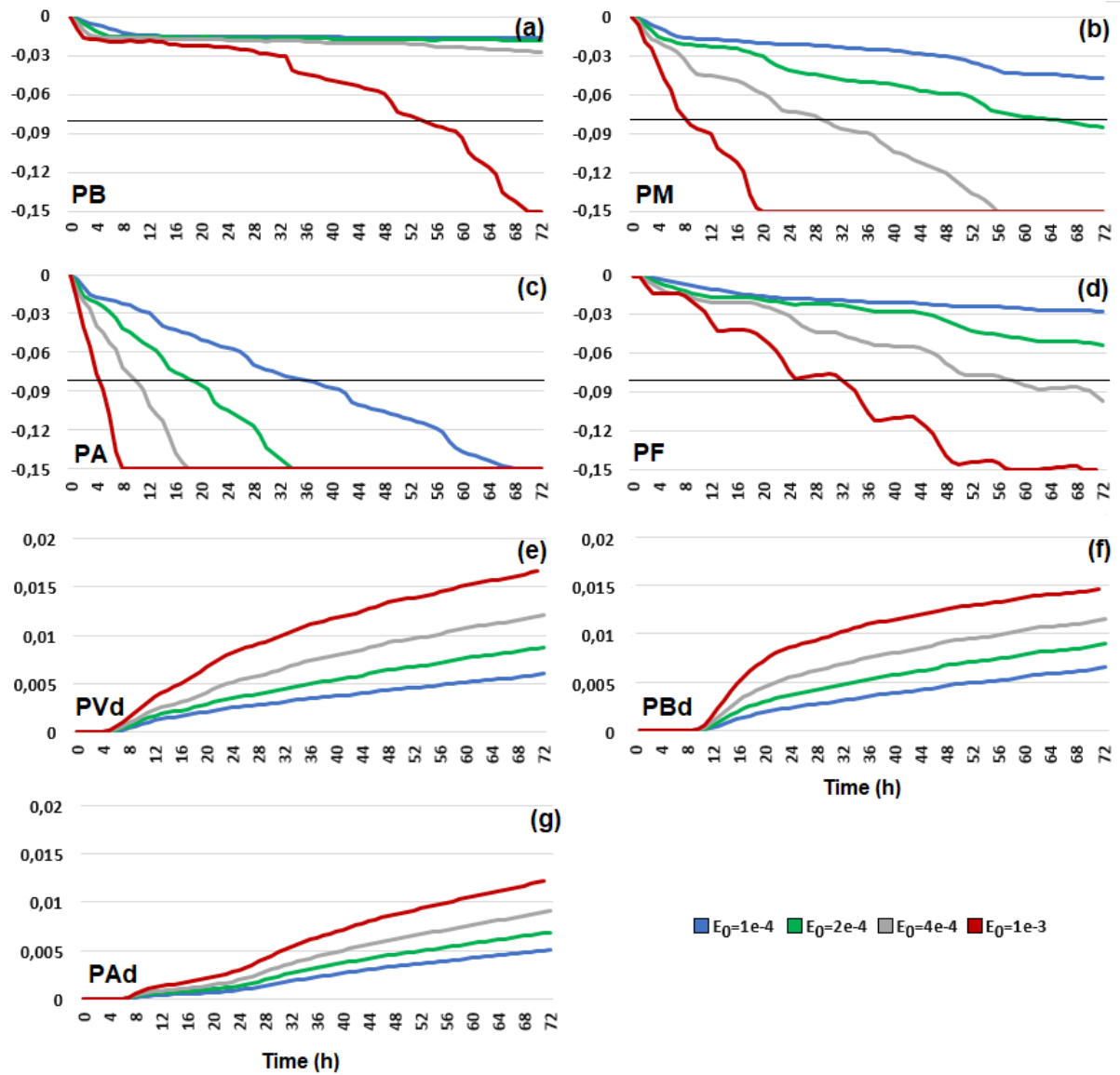

Fig. 13. Sensibility test on the erosion rate E_0 for N-NW wind of 21 m/s, for CF (coastal fraction case: 50% mud – 50% sand); (a-d) at PB, PA, PM and PF (black horizontal line corresponds to the erosion limit of 8cm acceptable for Z.n. restoration); (e-g) at PVd, PBd and PAd. Four E_0 values have been tested: $10^{-4}, 2*10^{-4}, 4*10^{-4}, 10^{-3}$ kg/m^2/s. Results corresponding to $E_0 = 10^{-3}$ kg/m^2/s (red curves in Figs.13a-d) may be compared with those shown in Fig.6a for $E_0 = 10^{-3}$ kg/m2/s and the initial composition (25% fine sand, 25% very fine sand, 25% coarse silt, 25% medium silt).

Table 1. Sediment composition and characteristics.

	Medium silt	Coarse silt	Very fine sand	Fine sand
Particle diameter (µm)	20	40	80	160
BSS_{cr} (N/m^2)	0.070	0.088	0.120	0.160
Particle density (kg/m^3)	2650	2650	2650	2650
Initial fraction in sediment (%)	25	25	25	25
Settling velocity W_s (m/s)	constant estimated from Stokes law: 0.000928	constant estimated from Stokes law: 0.000232	Soulsby formulation (1997): 0.017063	Soulsby formulation (1997): 0.004741
E_0 (kg/m^2/s)	10^{-3}	10^{-3}	10^{-3}	10^{-3}

Table 2. Parameters of the sensibility tests.

	1µm clay fraction (%)	20 µm medium silt fraction (%)	50µm coarse silt fraction (%)	200µm fine sand fraction (%)
DF	20	30	40	10
CF	10	15	25	50
BSS_{cr} (N/m^2)	0.005	0.046	0.1	0.175